



Joint modeling of lithosphere and mantle dynamics elucidating lithosphere-mantle coupling

A. Ghosh,¹ W. E. Holt,¹ L. Wen,¹ A. J. Haines,² and L. M. Flesch³

Received 2 May 2008; revised 14 June 2008; accepted 9 July 2008; published 27 August 2008.

[1] We provide new insights into the lithosphere-mantle coupling problem through a joint modeling of lithosphere dynamics and mantle convection and through comparison of model results with the high resolution velocity gradient tensor model along the Earth's plate boundary zones. Using a laterally variable effective viscosity lithosphere model, we compute depth integrated deviatoric stresses associated with both gravitational potential energy (GPE) differences and deeper mantle density buoyancy-driven convection. When deviatoric stresses from horizontal basal tractions, associated with deeper density buoyancy-driven convective circulation of the mantle, are added to those from GPE differences, the fit between the model deviatoric stress field and the deformation indicators improves dramatically in most areas of continental deformation. We find that the stresses induced by the horizontal tractions arising from deep mantle convection contribute approximately 50% of the magnitude of the Earth's deviatoric lithospheric stress field. We also demonstrate that lithosphere-asthenosphere viscosity contrasts and lateral variations within the lithospheric plate boundary zones play an important role in generating the right direction and magnitude of tractions that yield an optimal match between deviatoric stress tensor patterns and the deformation indicators. **Citation:** Ghosh, A., W. E. Holt, L. Wen, A. J. Haines, and L. M. Flesch (2008), Joint modeling of lithosphere and mantle dynamics elucidating lithosphere-mantle coupling, *Geophys. Res. Lett.*, 35, L16309, doi:10.1029/2008GL034365.

1. Introduction

[2] The lithosphere-mantle coupling problem has been a controversial issue in geodynamics for the past few decades. The question that has divided the earth science community is the degree of coupling between deeper density buoyancy-driven mantle circulation and the lithosphere, and whether such coupling has a role to play in lithosphere dynamics. The methods for tackling this problem consist of either predicting the velocities of the surface plates or modeling the lithospheric stress field. If the initial plate-mantle coupling model is correct, then the predicted velocities will match the observed plate motions and the modeled stress field will match the stress observations. Here, we investigate

the problem of lithosphere-mantle coupling by modeling the lithospheric stress field and comparing our results with strain rate tensor observations from the Global Strain Rate Map (GSRM) [Kreemer *et al.*, 2003].

[3] We address two principal sources of stress within the lithosphere: (1) internal buoyancy forces arising from lateral density variations within the lithosphere (lithosphere buoyancy) and (2) basal tractions associated with large-scale mantle convection arising from deeper density buoyancies below the lithosphere (mantle buoyancy). Bai *et al.* [1992] and Bird [1998], and more recently Steinberger *et al.* [2001] and Lithgow-Bertelloni and Gynn [2004], have modeled the lithospheric stress field by combining the above two sources. In most of these studies, the modeled stress field was compared with stress observations from the World Stress Map (WSM) [Zoback, 1992; Reinecker *et al.*, 2005]. One of the factors that distinguishes our study is a quantitative comparison of the modeled deviatoric stress tensor field with the GSRM's horizontal deformation tensor field within the Earth's plate boundary zones as well as a sensitivity analysis on the role of lithosphere-asthenosphere viscosity contrasts in generating the optimal magnitude of tractions at a reference level, taken as the generalized base of the lithosphere. In this paper we use a long-wavelength traction field generated by a simple convection model. The aim of our study is to investigate the joint contribution of internal lithospheric density buoyancies and these long-wavelength tractions on the deviatoric stress field of the lithosphere.

2. Method

[4] Internal buoyancy sources within the lithosphere influence the lithospheric stress field by giving rise to gravitational potential energy (GPE) differences, which in turn produce deviatoric stresses. Density buoyancy-driven mantle convection gives rise to basal tractions that act upon the base of the lithosphere to yield a contribution to deviatoric stresses. We use the thin sheet approximation to solve for vertically integrated deviatoric stresses associated with both of these effects. This involves vertically integrating the force-balance equations from a reference level at radius r_L to the Earth's surface, radius r_S (see Text S1¹, Appendix A). The level of integration, r_L , is taken to be a constant depth of 100 km below the sea-level. Note that r_S varies in continents due to variable surface topography, whereas in oceans r_S constitutes the sea-level and is thus constant.

[5] Solutions to the force-balance equations for the vertical integrals of horizontal deviatoric stress can be obtained

¹Department of Geosciences, Stony Brook University, Stony Brook, New York, USA.

²Department of Earth Sciences, University of Cambridge, Cambridge, UK.

³Department of Earth and Atmospheric Sciences, Purdue University, West Lafayette, Indiana, USA.

given GPE differences [e.g., *Flesch et al.*, 2001; *Ghosh et al.*, 2006]. Density buoyancy-driven mantle convection also produces radial and horizontal tractions that act at the bottom of the lithosphere. The radial tractions yield dynamic topography at the Earth's surface. The influence of this dynamic topography (or radial traction) on lithospheric stress can be dealt with in two ways. First, because the present-day topography already contains the dynamic contribution related to deep mantle convection, one can calculate the depth integrals of vertical stresses using the present-day topography and density structures in the lithosphere (the crustal and upper mantle structure in the top 100 km of the Earth). The depth integrals of vertical stresses following this procedure should be viewed as the summation of two components, with one contributed by the lithosphere buoyancies and the other by the radial tractions acting at the base of the lithosphere from the deep mantle density buoyancies. Such an approach does not address the consistency problem between the observed dynamic topography and predicted dynamic topography. In the present case, the densities in the lithosphere are obtained from the seismically inferred crustal structures (e.g., Crust 2.0 [G. Laske et al., Crust 2.0: A new global crustal model at 2×2 degrees, 2002, available at <http://mahi.ucsd.edu/Gabi/rem.html>]). Alternatively, one can directly compute the corresponding deviatoric stresses in the lithosphere from the predicted dynamic topography or radial tractions from the convection models. These deviatoric stresses are then added to those associated with a compensated lithosphere model. In such a treatment, the surface topography used to calculate the GPE difference in the lithosphere model is the compensated component based on the density buoyancies in the lithosphere. The deviatoric stress field produced by the compensated lithosphere model represents the contributions from only the density buoyancies in the lithosphere. If a convection model is self-consistent, that is, it predicts dynamic topography that matches, in both pattern and magnitude, the observed residual topography (total observed topography minus the compensated component) the above two approaches should yield same results. In this study, we adopt the first approach and address the self consistency of predicting dynamic topography in future studies.

[6] In order to obtain the deviatoric stresses associated with the horizontal tractions that are generated by density buoyancy-driven mantle flow, solutions to the force-balance equations can be calculated given distributions of the horizontal tractions (Text S1, Appendix A). The solution from horizontal tractions is then added to the solution from GPE differences described above to obtain the total deviatoric stress field. The suitability of the thin sheet approximation in the presence of large-scale three dimensional flow is discussed in Text S1, Appendix D.

[7] In our global model, we solve the force-balance equations on a $2.5^\circ \times 2.5^\circ$ global grid using a finite element technique [*Flesch et al.*, 2001] such that the deviatoric stress field solution provides a global minimum in the second invariant of deviatoric stress (Text S1, Appendix B).

[8] We calculate GPE from the crustal thickness and density dataset, Crust 2.0. The cooling plate model based on ocean floor age data [*Müller et al.*, 1997] with revised parameters from *Stein and Stein* [1992] is used to define densities for oceanic regions. The plate boundary zones are

assigned variable viscosities based on strain rates from the GSRM [*Kreemer et al.*, 2003] (see Text S1, Appendix B). We calculate GPE and the associated deviatoric stresses from the uncompensated Crust 2.0 model, which incorporates the contribution from radial tractions (dynamic topography) in addition to the contribution from lithosphere buoyancy sources.

[9] The horizontal tractions are derived from a convection model by *Wen and Anderson* [1997b] on solving the conservation equations of mass and momentum, using the constitutive equation between stress and strain rate with free slip boundary conditions, by a standard propagator matrix technique. Our mantle convection model is a whole mantle (WM) model with radially variable viscosities, the lower mantle being 10 times more viscous than the upper mantle. Unlike *Wen and Anderson* [1997b], we do not consider lateral viscosity variations within the lithosphere in our simple convection models. The density anomalies in the upper mantle are inferred by adjusting the relative weights of density anomalies related to subducting slabs [*Wen and Anderson*, 1995] and residual tomography [*Wen and Anderson*, 1997a], on the basis of fitting the geoid. The density structure in the lower mantle was derived from a seismic tomographic model [*Su et al.*, 1994]. The detailed information for the density model and the velocity density scalings were presented by *Wen and Anderson* [1997b]. The contributions that the horizontal tractions make on the lithospheric deviatoric stress field are computed using the thin sheet model with laterally variable viscosity. The negative of these horizontal tractions, or body force equivalents, are applied at the base of the variable viscosity thin sheet as a boundary condition (see Text S1, Appendix A). The contribution from the basal tractions is then added to the contribution from GPE differences to determine a total horizontal deviatoric stress field.

3. A Quantitative Comparison With Deformation Indicators at Plate Boundary Zones

[10] We test our modeled deviatoric stresses quantitatively with strain indicators from the GSRM [*Kreemer et al.*, 2003]. GSRM is a high resolution model based on 5170 GPS stations and Quaternary fault slip data, confined along the deforming plate boundary zones. The modeled deviatoric stress tensors are scored with the strain rate tensors in GSRM, and we seek to match direction of principal axes as well as style of faulting inferred from the strain rate tensors. We define a correlation coefficient [*Flesch et al.*, 2007]:

$$-1 \leq \sum_{\text{areas}} (\varepsilon \cdot \tau) \Delta S / \left(\sqrt{\sum_{\text{areas}} (E^2) \Delta S} * \sqrt{\sum_{\text{areas}} (T^2) \Delta S} \right) \leq 1 \quad (1)$$

where $E = \sqrt{\varepsilon_{\phi\phi}^2 + \varepsilon_{\theta\theta}^2 + \varepsilon_{rr}^2 + \varepsilon_{\phi\theta}^2 + \varepsilon_{\theta\phi}^2} = \sqrt{2\varepsilon_{\phi\phi}^2 + 2\varepsilon_{\phi\theta}\varepsilon_{\theta\phi} + 2\varepsilon_{\theta\theta}^2 + 2\varepsilon_{rr}^2}$, $T = \sqrt{\tau_{\phi\phi}^2 + \tau_{\theta\theta}^2 + \tau_{rr}^2 + \tau_{\phi\theta}^2 + \tau_{\theta\phi}^2} = \sqrt{2\tau_{\phi\phi}^2 + 2\tau_{\phi\theta}\tau_{\theta\phi} + 2\tau_{\theta\theta}^2 + 2\tau_{rr}^2}$ and $\varepsilon \cdot \tau = 2\varepsilon_{\phi\phi}\tau_{\phi\phi} + \varepsilon_{\phi\theta}\tau_{\theta\theta} + \varepsilon_{\theta\theta}\tau_{\phi\phi} + 2\varepsilon_{\theta\theta}\tau_{\theta\theta} + 2\varepsilon_{\phi\theta}\tau_{\phi\theta}$. E and T are the second invariants of strain rate and stress, ε_{ij} are strain rates from *Kreemer et al.* [2003], ΔS is the grid area, and τ_{ij} are the calculated deviatoric stresses. Normalization by E and T ensures that the correlation coefficient depends only on the inferred style of faulting embedded in the

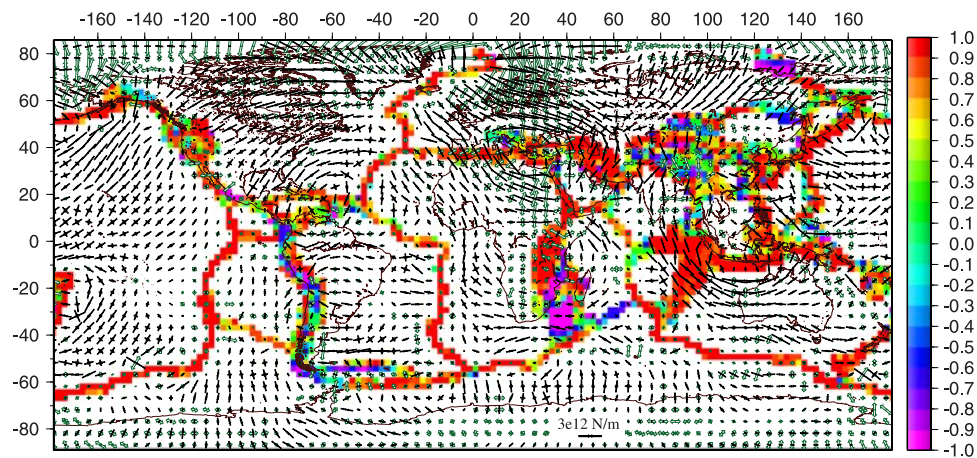


Figure 1. Global distribution of vertically integrated horizontal deviatoric stresses and correlation coefficients (on scale bar, equation 1) between observed strain rate tensors from the GSRM and deviatoric stress tensors arising from GPE differences from the Crust 2.0 model. Tensional deviatoric stresses are shown by green arrows while compressional deviatoric stresses are shown by black arrows. Length of the arrows are proportional to the magnitude of stresses. Strike-slip regions are indicated by one tensional and one compressional pair of arrows.

deviatoric stress and strain rate tensors and on the direction of principal axes of strain rate and stress tensors; there is no dependence on magnitude of stress or strain rate. The maximum correlation coefficient of +1 indicates a perfect fit between the directions of principal axes of deviatoric stress and directions of principal axes of strain rate as well as a perfect fit between expected styles of faulting associated with the deviatoric stress and strain rate tensors. The minimum coefficient of -1 indicates anti-correlation. A value of 0 implies no fit, including, for example, predicted strike-slip style of deviatoric stress, where the compressional and tensional principal axes differ from those in the GSRM by 45° .

4. Results

4.1. Deviatoric Stresses From GPE Differences

[12] There occurs a positive correlation between higher elevation areas and areas of high GPE, such as Andes, western North America, and the Tibetan Plateau. These high GPE areas are also in deviatoric tension. Topographically low areas and older oceans exhibit low GPE and conse-

quently are in deviatoric compression (Figures 1 and S2). Comparison of modeled stresses from GPE differences to the deformation indicators in GSRM indicates an excellent fit along the mid-oceanic ridges and the Indo-Australian boundary zone. Areas of continental deformation, such as western North America, Andes and central Asia, exhibit a poor fit (Table 1 and Figure 1), clearly indicating that in those areas, lateral variations in GPE are not sufficient to explain the observed deformation.

4.2. Total Deviatoric Stress Field From Combined GPE Differences and Mantle Buoyancies

[13] In the mantle convection models used to generate horizontal basal traction estimates, we test a range of lithosphere viscosities from slightly strong (5×10^{21} Pa-s) to very strong (100×10^{21} Pa-s) (Figure 2). The asthenosphere viscosity is also varied by 4 orders of magnitude, from 10^{18} to 10^{21} Pa-s. Amongst the various models of radially symmetric viscosity structures that we test, the ones marked within the ellipse generate deviatoric stresses, which when added to the deviatoric stresses from GPE differences (Figure 1), yield global correlation coefficients with GSRM

Table 1. Correlation Coefficients Obtained From a Comparison Between Different Deviatoric Stress Models With the Strain Rate Tensor Field From the GSRM Model^a

Region of Interest	Number of Areas	GPE Differences With Rheological Variations	GPE Differences Plus Basal Tractions	GPE Differences With Constant Viscosity	GPE Differences Plus Basal Tractions
W. North America	132	0.53	0.64	0.08	0.11
Andes	89	0.24	0.84	-0.20	0.78
Eastern Africa	164	0.32	0.76	0.63	0.81
Mediterranean	83	0.55	0.57	0.33	0.39
Central Asia	187	0.33	0.57	0.10	0.29
Indo-Australian plate boundary zone	174	0.69	0.76	0.30	0.31
Mid-oceanic ridges	292	0.80	0.85	0.78	0.76
Western Pacific	109	0.51	0.63	0.08	0.61
South East Asia	167	0.61	0.66	0.08	0.34
Total	1944	0.54	0.69	0.31	0.48

^aSee equation (1). The mantle viscosity model considered is model 8. The viscosities in the lithosphere of the thin sheet model vary as function of strain rates (Figure S1) for columns 3 and 4, whereas for the last two columns, the lithosphere in the thin sheet model has uniform viscosity.

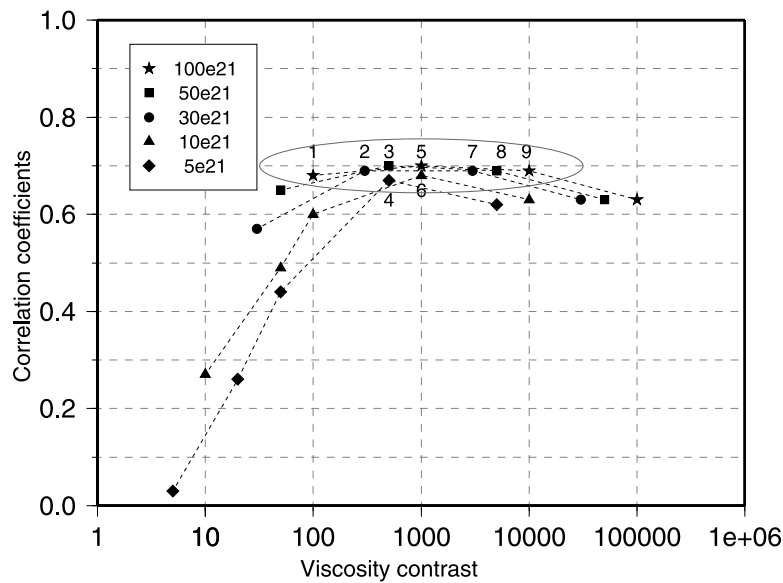


Figure 2. Viscosity contrast between lithosphere and asthenosphere vs. correlation coefficients. The different symbols indicate lithosphere of different strengths. The models within the ellipse yield correlation coefficients greater than 0.65. Viscosities are given in Pa-s.

of 0.65 and above. One aspect common to all these models is the need for a strong viscosity contrast between the lithosphere and the asthenosphere (100–10,000 times stronger lithosphere). All successful models (1–9) yield a consistent long-wavelength pattern of horizontal tractions acting at 100 km depth (see Figure S3).

[14] Viscosity models 1–5 (with a lithosphere-asthenosphere viscosity contrast between 100 and 1000) yield horizontal tractions at 100 km depth that are of magnitude 3–6 MPa (Figure S4), and provide horizontal deviatoric stresses that dominate stresses associated with GPE differences (Figure S5a). Close inspection suggests that these models are less than optimal because they predict thrust faulting in parts of Tibet and Lake Baikal regions, and too little tension in the U.S. Basin and Range and the Aegean region.

Viscosity models 6–9 (with a lithosphere-asthenosphere viscosity contrast between 1000 and 10000 and with a weak asthenosphere of 10^{19} Pa-s), on the other hand, yield deviatoric stress magnitudes closer to stress magnitudes from GPE differences (Figure S5b) and provide a more favorable match to deformation indicators in the above mentioned regions. Models 6–9 are thus our preferred models. The horizontal tractions from models 6–9 have the same pattern as models 1–5, but the magnitudes are reduced, and range between 1–2.5 MPa (Figure S3). Deviatoric stresses from the combined sources of GPE differences and horizontal tractions from mantle buoyancies (Figure 3) show improvement of fitting in all areas, particularly in regions of continental deformation (Table 1 and Figure 3). Viscosity models with too small a contrast

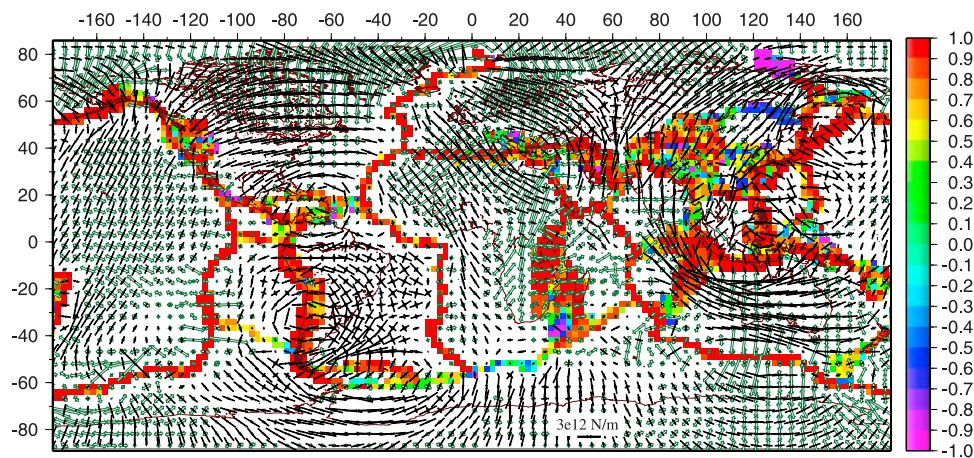


Figure 3. Global distribution of total vertically integrated horizontal deviatoric stresses obtained from GPE differences (Figure 1) and horizontal tractions combined, plotted on correlation coefficients between these total deviatoric stress tensors and strain rate tensors from the GSRM. The mantle convection model is a radially variable viscosity model with a strong lithosphere (50×10^{21} Pa-s) and a weak asthenosphere (10^{19} Pa-s) (model 8).

between the lithosphere and asthenosphere (models outside the ellipse) yield a poor fit to the deformation indicators (Figures 2 and S6).

[15] While a uniform viscosity lithosphere in the thin sheet model still improves the fit to the strain rate tensor information when the mantle contribution is added to the lithospheric contribution, the overall fit is much lower than when lateral variations are present (Table 1). The inferred lateral viscosity variations in the lithosphere above, however, have little effects on the large scale basal tractions generated by the deep convection models. For example, we compute degree 12 and degree 20 convection model responses using the lithospheric viscosity structure of the thin sheet and find that tractions from these models (Figure S7) have little difference from those of the uniform lid lithosphere model (Figure S8). Therefore, for simplicity in the present study, we have adopted large scale convection models with a uniform viscosity lithospheric lid. Some other types of lateral variation of viscosity in the lithosphere (for example, the continent and ocean divide) would have large effects on the large scale tractions from deep mantle circulation [Wen and Anderson, 1997b]. We will address this issue in a future study with the observed plate motion as a further constraint.

5. Discussion and Conclusion

[16] Our results show that deviatoric stresses from GPE differences alone are not able to match the direction of principal axes and style of faulting in many of the deformation zones of the Earth's surface, particularly within the continental zones of deformation; horizontal basal tractions arising from mantle convection are also required to match the deformation indicators. These horizontal basal tractions that are coupled to the base of the lithospheric plates arise from mantle flow induced by current and past subducted lithosphere in these areas (e.g., the Indian plate, Andes, Figure S3). An aspect that is of prime importance is the viscosity contrast between the lithosphere and the asthenosphere, where a sufficiently large contrast (100–10,000 times) is required for the effective body forces associated with horizontal tractions to have the right directions and magnitudes. Although a wide range of models involving viscosity contrasts between lithosphere and asthenosphere appear to adequately match the global GSRM data (models 1–9), our preferred models are those in which horizontal tractions and GPE differences contribute approximately equally to the deviatoric stress field. These models (6–9) involve a weak asthenosphere of 10^{19} Pa-s, horizontal traction magnitudes of 1–2.5 MPa, and vertically integrated compressional deviatoric stress magnitudes ranging between $1-4 \times 10^{12}$ N/m, consistent with deviatoric stress magnitudes obtained by Richardson [1992]. Lateral viscosity variations within the plate boundary zones improve the fit to the deformation indicators there, although these lateral variations have little effect on the large-scale basal traction patterns that are

generated by the deep convection models. In future studies we will address other types of lateral variation of viscosity in the lithosphere, such as the continent and ocean divide, which have significant effects on the large scale tractions from deep mantle circulation [Wen and Anderson, 1997b].

[17] **Acknowledgments.** This work benefited considerably from reviews provided by Peter Bird, Bernhard Steinberger and an anonymous reviewer. Maps were prepared using GMT version 3.4.4 by P. Wessel and W.F. Smith, and the work was supported by NSF grant EAR-0310193 and a NASA grant NNG04GQ17G.

References

- Bai, W., C. Vigny, Y. Ricard, and C. Froidevaux (1992), On the origin of deviatoric stresses in the lithosphere, *J. Geophys. Res.*, *97*, 11,729–11,737.
- Bird, P. (1998), Testing hypotheses on plate-driving mechanisms with global lithosphere models including topography, thermal structure and faults, *J. Geophys. Res.*, *103*, 10,115–10,129.
- Flesch, L. M., A. J. Haines, and W. E. Holt (2001), Dynamics of the India-Eurasia collision zone, *J. Geophys. Res.*, *106*, 16,435–16,460.
- Flesch, L. M., W. E. Holt, A. J. Haines, L. Wen and B. Shen-Tu (2007), The dynamics of western North America: Stress magnitudes and the relative role of gravitational potential energy, plate interaction at the boundary, and basal tractions, *Geophys. J. Int.*, *169*, 866–896.
- Ghosh, A., W. E. Holt, A. J. Haines, and L. M. Flesch (2006), Gravitational potential energy of the Tibetan Plateau and the forces driving the Indian plate, *Geology*, *34*, 321–324.
- Kreemer, C., W. E. Holt, and A. J. Haines (2003), An integrated global model of present-day plate motions and plate boundary deformation, *Geophys. J. Int.*, *154*, 8–34.
- Lithgow-Bertelloni, C., and J. H. Guynn (2004), Origin of the lithospheric stress field, *J. Geophys. Res.*, *109*, B01408, doi:10.1029/2003JB002467.
- Müller, R. D., W. Roest, J. Royer, L. Gahagan, and J. Sclater (1997), Digital isochrons of the world's ocean floor, *J. Geophys. Res.*, *102*, 3211–3214.
- Reinecker, J., O. Heidbach, M. Tingay, B. Sperner, and B. Müller (2005), The release 2005 of the World Stress Map, Geophys. Inst., Karlsruhe Univ., Karlsruhe, Germany. (Available at www.world-stress-map.org)
- Richardson, R. M. (1992), Ridge forces, absolute plate motions, and the intraplate stress field, *J. Geophys. Res.*, *97*, 11,739–11,748.
- Stein, C. A., and S. Stein (1992), A model for the global variation in oceanic depth and heat flow with lithospheric age, *Nature*, *1992*, 123–129.
- Steinberger, B., H. Schmeling, and G. Marquart (2001), Large-scale lithospheric stress field and topography induced by global mantle circulation, *Earth Planet. Sci. Lett.*, *186*, 75–91.
- Su, W. J., R. L. Woodward, and A. M. Dziewonski (1994), Degree 12 model of shear velocity heterogeneity in the mantle, *J. Geophys. Res.*, *99*, 6945–6980.
- Wen, L., and D. L. Anderson (1995), The fate of the slabs inferred from seismic tomography and 130 Ma subduction, *Earth Planet. Sci. Lett.*, *133*, 185–198.
- Wen, L., and D. L. Anderson (1997a), Slabs, hotspots, cratons and mantle convection revealed from residual seismic tomography in the upper mantle, *Phys. Earth Planet. Int.*, *99*, 131–143.
- Wen, L., and D. L. Anderson (1997b), Present-day plate motion constraint on mantle rheology and convection, *J. Geophys. Res.*, *102*, 24,639–24,653.
- Zoback, M. L. (1992), First and second order patterns of stress in the lithosphere: The World Stress Map Project, *J. Geophys. Res.*, *102*, 11,703–11,728.

L. M. Flesch, Department of Earth and Atmospheric Sciences, Purdue University, West Lafayette, IN 47907-2051, USA.

A. Ghosh, W. E. Holt, and L. Wen, Department of Geosciences, Stony Brook University, Stony Brook, NY 11790, USA. (aghosh@mantle.geo.sunysb.edu)

A. J. Haines, Department of Earth Sciences, University of Cambridge, Cambridge CB2 3EQ, UK.